geoconvention
Calgary • Canada • May 11-13 2026

Implementation of fast chirp-z Radon transform for demultiple and deblending

E. Jair Zampieri [1], *Joaquín Acedo* [1], *Mauricio D. Sacchi* [1]

[1] *Signal Analysis and Imaging Group (SAIG), Department of Physics, University of Alberta*

Summary

The Radon transform has been widely used in various areas of seismology. Achieving a fast, high-resolution transform often requires multiple applications of the forward and adjoint operators, making the development of computationally efficient algorithms a priority. In particular, the classic implementation of the parabolic Radon transform in the frequency domain has a computational complexity of $\mathcal{O}(N_f N_x N_p)$. The variant proposed in this paper redefines the kernel in a new domain where its sparsity is maximized. This approach enables a more efficient transform computation, reducing the complexity to $\mathcal{O}(N_f N_x \log N_x)$. The reduction represents a significant improvement and streamlines applications to large datasets. The efficiency of the new transform relies on its ability to return to its original domain by sampling only the necessary coefficients per frequency slice using the chirp-z transform. This technique offers computational advantages by rearranging the terms into a convolution form. Additionally, the lack of constraints on spatial sampling makes this method particularly well-suited for seismic data reconstruction in scenarios with irregular trace coverage. Numerical tests are conducted to evaluate the performance of the new transform relative to the traditional and other fast frequency-domain approaches. Examples of multiple attenuation and deblending by denoising are also presented.

Introduction

Radon transforms are applied widely in seismology. In particular, the linear Radon transform (LRT) and the parabolic Radon transform (PRT) are both relevant for their relatively low computational cost. These are commonly referred to as time-invariant Radon transforms because their basis functions are invariant under time shifts and they can be efficiently implemented in the frequency domain.

The LRT has been applied in several important areas of exploration seismology after its first introduction in 1917 (Radon, 1917). Some examples are plane-wave decomposition and ground-roll attenuation (Stoffa et al., 1981; Tatham et al., 1983), multiple attenuation via predictive deconvolution (Treitel et al., 1982), inversion of common-midpoint data (Stoffa et al., 1981), and Rayleigh-wave separation and group velocity estimation (Luo et al., 2009; Askari and Hejazi, 2015). On the other hand, the PRT was introduced by Hampson (1986) and has been especially effective for multiple attenuation (Foster and Mosher, 1992; Herrmann et al., 2000) and offset interpolation (Darche, 1990; Trad et al., 2002). The PRT is sometimes preferred over the hyperbolic variant since it is less computationally intensive. Applications of PRT can be effective with time-stretched and moveout-corrected data (Yilmaz, 1989; Hampson, 1986). More recent applications use variants of linear and parabolic RT to separate erratic noise from data in the context of deblending by denoising (Ibrahim and Sacchi, 2014).

At its core, the Radon transform projects data by summing along specific curves in the time-space domain and mapping the result into a new space, the Radon domain. Events in this new domain are compressed and map to different regions than the noise, enabling separation by filtering. In 3D data, these summations are applied over surfaces rather than curves. For the time-invariant case,

the general form of the transform is given by

$$t = \tau + p\varphi(x) \tag{1}$$

where $\varphi(x)$ defines the curvature of the summation path. The LRT uses $\varphi(x) = x$, while the PRT defines $\varphi(x) = x^2$. Hyperbolic Radon transforms are also used, employing the relation $t = \sqrt{\tau^2 + px^2}$.

As previously mentioned, the key goal of Radon transforms is to compress the event to enable separation from noise in the Radon domain. However, practical limitations, such as spatial sampling and the aperture of seismic surveys, lead to a high correlation between Radon basis functions and a non-orthogonal transform (Gholami and Zand, 2017). Consequently, solvers such as Conjugate Gradients (CG) are commonly employed to cast the transforms as a damped least-squares problem (Hampson, 1986; Kostov, 1990; Beylkin, 1987). Moreover, sparse-promoting inversion strategies are often used to improve the focus of events in the Radon domain, leading to the high-resolution Radon transform and its variants (Sacchi and Ulrych, 1995).

This report presents an improved implementation of the frequency-domain RT kernel. In our implementation, the matrix used for each slice is computed in the Fourier domain, where it is sparest, thereby drastically reducing computational cost (Gholami and Zand, 2017; Gholami and Farshad, 2019). Despite being frequency-dependent, the kernel is initially computed for all frequencies and then efficiently recovered at each frequency slice using the chirp-z transform Rabiner et al. (1969); Proakis (2001).

Radon transform

When using the Radon transform, we model the seismic signal $u(x,t)$ as a superposition of events. The operator R is typically non-orthogonal, leading to the smearing observed in the low-resolution adjoint $R^{\mathrm{H}}u$. To overcome this, we seek a sparse solution v that minimizes

$$\min_{v} \ \|Rv - u\|_2^2 + \mu\|v\|_1, \tag{2}$$

where the ℓ_1 norm encourages a compact representation in the Radon domain. Solving this iteratively requires multiple applications of both the forward and adjoint operators, thereby necessitating a fast kernel implementation.

Fast implementation in the frequency domain

The frequency domain allows us to treat each frequency slice independently. Introducing the combined index $\lambda_j = k\gamma_j$, we redefine the kernel $S_{n,j}$ as

$$S_{n,j} = e^{i2\pi\Delta f\Delta p\,\varphi(x_n)k\gamma_j} \rightarrow S_{n,j} = e^{i2\pi\Delta f\Delta p\,\varphi(x_n)\lambda_j} \tag{3}$$

Then, for a fixed x_n, this kernel is a mono-frequency complex exponential. When we apply a DFT along the λ dimension, the energy becomes highly localized.

By making an order of magnitude comparison, we can discard the imaginary part and work only with the real part of the Fourier-transformed kernel $\hat{S}_{n,l}$. This yield

$$S_{n,j} \approx \frac{(-1)^l}{N_\lambda}\sin(N_\lambda\pi\theta_n)\cot\left(\pi[\theta_n - \frac{l}{N_\lambda}]\right), \qquad \text{where } n = \Delta p\Delta f\,\varphi(x_n).$$

(4)

When analyzing this expression, we can see the high level of sparsity. This is one of the key advantages of the algorithm, as it allows for a fast implementation of the kernel. By applying a threshold, we can zero out nearly 99% of the matrix without significant loss of information. This changes the dense matrix-vector multiplication into a sparse operation, drastically reducing the number of complex multiplications per frequency slice. A primary challenge in this fast formulation is that the frequency k serves as a scaling factor for sampling the λ axis (used for the Fourier transform along the rows of S). A standard inverse Fourier transform is insufficient because it cannot accommodate the frequency-dependent spacing required to recover $\hat{v}_{k,j}$.

We utilize the identity $j_l = \frac{1}{2}[l^2 + j^2 - (j-l)^2]$ to recast the transform as a discrete convolution using the Bluestein algorithm. This allows us to use the FFT to perform the mapping:

$$\hat{v}_{k,j} = \hat{c}_{k,j} \sum_{l=0}^{N_l-1} \hat{V}_{k,l}\, \hat{b}_{k,l}\, h_{k,j-l}.$$

The implementation relies on three precomputed phase-shift operators $(\hat{a}, \hat{b}, \hat{c})$ and the chirp signal h.

$$\hat{V}_{k,l} = \hat{c}_{k,j} \sum_{l=0}^{N_l-1} \hat{V}_{k,l}\, \hat{b}_{k,l}\, h_{k,j-l}.$$

Algorithmic Implementation and Complexity

The total workflow for the fast adjoint operator $\mathbf{R}^{\mathrm{H}}$ is summarized as follows:

1. FFT: transform input data $\mathbf{u} \rightarrow \hat{\mathbf{u}}$.
2. Phase shift: apply precomputed operators $\hat{\mathbf{u}} \cdot \hat{\mathbf{a}}$.
3. Sparse mapping: multiply by sparse kernel $\hat{S}$.
4. Perform the FFT-based convolution with chirp signal $\mathbf{h}$ and apply weights $\hat{\mathbf{b}}$, $\hat{\mathbf{c}}$.
5. IFFT: return to time domain.

This leads to the following compact formulation for the adjoint operator:

$$\begin{aligned}\hat{\mathbf{v}} &= \hat{\mathbf{c}} \left[\cdot(\hat{\mathbf{u}} \cdot \hat{\mathbf{a}})\, \hat{\mathbf{S}} \cdot \hat{\mathbf{b}} *_l \mathbf{h}\right] \\ &= \hat{\mathbf{c}} \cdot \mathrm{IFFT}\left[\mathrm{FFT}\left[(\hat{\mathbf{u}} \cdot \hat{\mathbf{a}})\, \hat{S} \cdot \hat{\mathbf{b}}\right] \cdot \hat{\mathbf{h}}\right]\end{aligned}$$

where $\hat{\mathbf{h}}$ is the Fourier transform of $\mathbf{h}$ along the second dimension, associated with the parameter l. Considering the adjoint of each operator, the direct Radon transform can be written as:

$$\hat{\mathbf{u}} = \hat{\mathbf{b}}^* \cdot \mathrm{IFFT}\left[\mathrm{FFT}(\hat{\mathbf{v}} \cdot \hat{\mathbf{c}}^*) \cdot \hat{\mathbf{h}}^*\right] \hat{S}^T \cdot \hat{\mathbf{a}}^* \tag{5}$$

The standard frequency-domain approach scales with $\mathcal{O}(N_f N_x N_p)$. The proposed method scales with $\mathcal{O}(N_f N_x \log N_x)$, representing an order-of-magnitude improvement.

Results

The performance of the fast transform (forward and adjoint) is tested for a specific frequency slice, in this case $f_k = 1Hz$, and compared with the classic Radon transform in the frequency domain and the Toeplitz application presented by Sacchi and Porsani (1999). The algorithms were tested across different dataset sizes, with equal lengths for the Radon parameter and the offset ($N = N_p = N_x$).

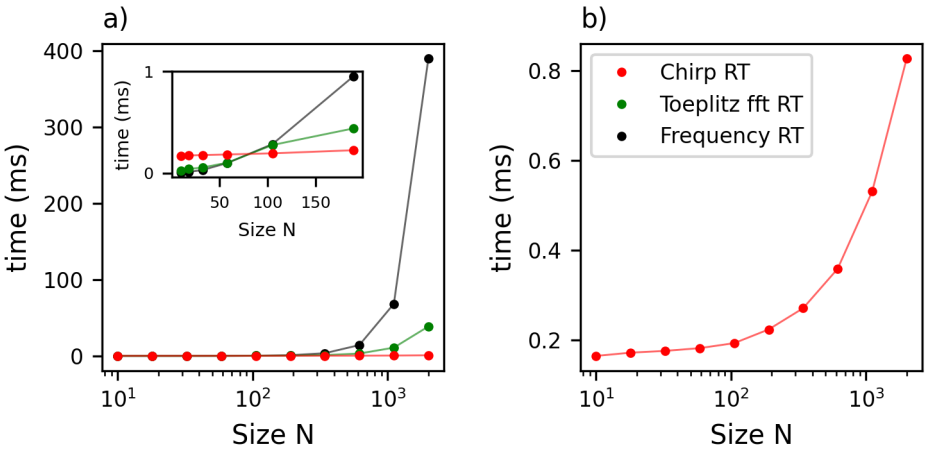


Figure 1: Comparison of the time required to compute the fast Radon transform (in red), the classic frequency domain application (in black) and the Toeplitz implementation (in green) for the frequency slice $f_k = 1\ Hz$.

The times shown in Figure 1 demonstrate the superior efficiency of the presented algorithm. While the computational cost is lower for smaller problems in the frequency RT, the relationship reverses after the dataset exceeds approximately 70 samples. For large problems, the difference increases considerably, especially when compared with the classic Radon transform. For a dataset of 2000 samples, the operation takes 0.8 ms for the fast Radon transform, 38.00 ms for the regular frequency Radon transform and 390 ms for the classic Radon transform.

The results in Figure 2a-c demonstrate the expected compression of the data in the Radon domain, where the energy is focused into four distinct peaks, with smearing due to the limited aperture and sampling. Then, the back projection demonstrates a proper recovery of the signals and noise reduction on the background. The signal shows better resolution with iterative solvers, particularly with FISTA, compared to direct application of the operator. This is consistent with the application of sparse-promoting iterative algorithms and data misfit reduction. It is important to highlight that these solvers are applied in each frequency slice; therefore, the compression is not forced along the τ-axis.

To demonstrate the effectiveness of the proposed method in signal separation tasks, we applied the algorithm to a real CMP gather from the Mississippi Canyon, Gulf of Mexico (Figure 3). The original data (Figure 3a) exhibits strong multiple energy that interferes with the primary reflections. The high-resolution Radon panel 3, computed using the fast sparse algorithm, successfully distinguishes these events based on their residual moveout, focusing the energy into distinct, compact clusters. By muting the coefficients associated with the multiple energy and applying the forward transform, we recover

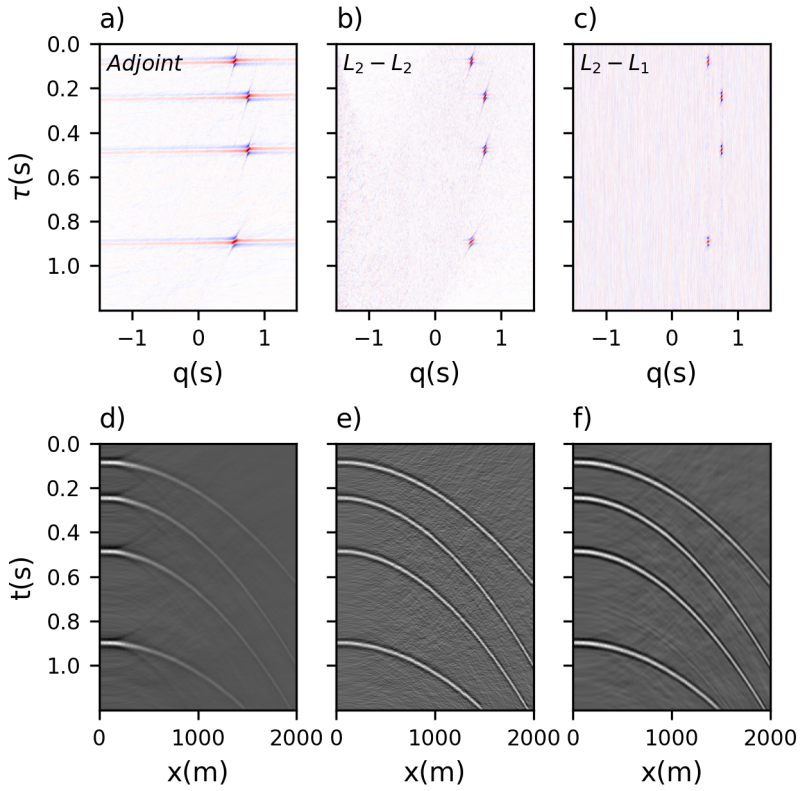


Figure 2: Application of the adjoint operator (a), the Conjugate Gradients solver (b) and the FISTA solver (c) for the projection to the Radon transform and then back-projected to the data domain using the forward operator (d,e,f).

the estimated primaries (Figure 3c). The result shows significant suppression of the multiples while preserving the primary signal character, validating the transform's ability to handle field data with complex amplitude variations.

Finally, we evaluate the method's effectiveness in a deblending scenario (Figure 4). The fast Radon operator is applied to a Common Receiver Gather (CRG) contaminated with blending noise. The blending factor is $\beta = 2$. By enforcing sparsity in the misfit term, the erratic noise is removed, while the hyperbolic events are modelled using the Radon operator. The reconstructed 'Predicted CRG' (Figure 4b) shows clean signal continuity, while the 'Difference' panel (Figure 4c) confirms that the removed energy consists almost exclusively of incoherent interference, demonstrating the algorithm's suitability for large-scale deblending tasks. Denoising was applied using 3 windows, each divided along the offset axis. The border windows used a linear fast Radon transform, and the one in the middle applied the parabolic form with apex shift. The result was obtained using a Conjugate Gradients solver within an IRLS scheme, updating the weights to minimize the misfit at each iteration.

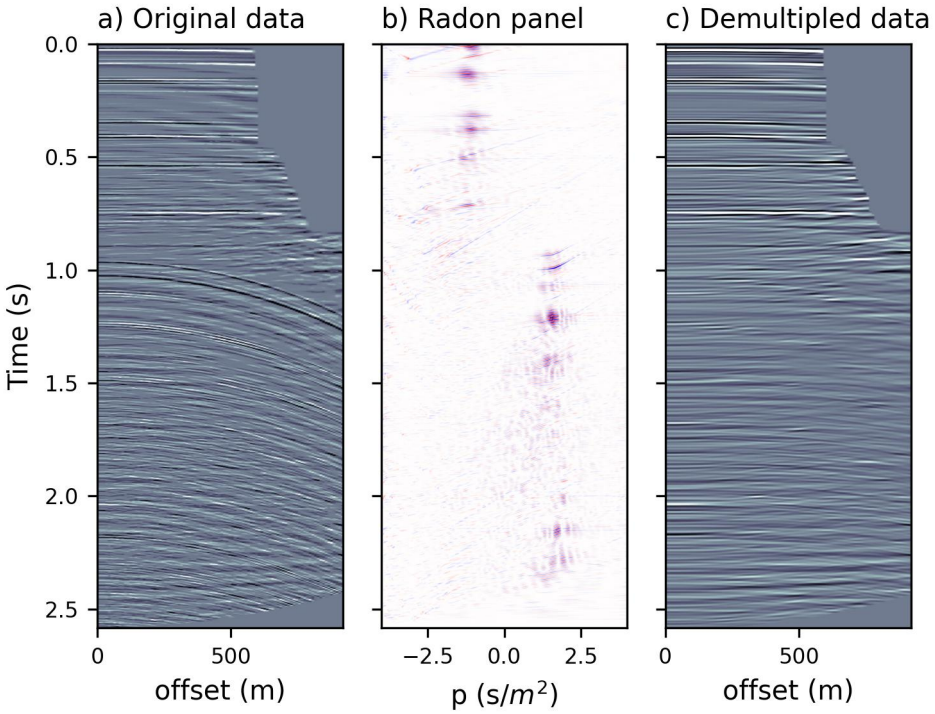


Figure 3: CMP gather from the Gulf of Mexico (Mississippi Canyon dataset). b) Radon panel obtained from the high-resolution Fast parabolic Radon transform. c) The estimated primaries with multiple mitigated.

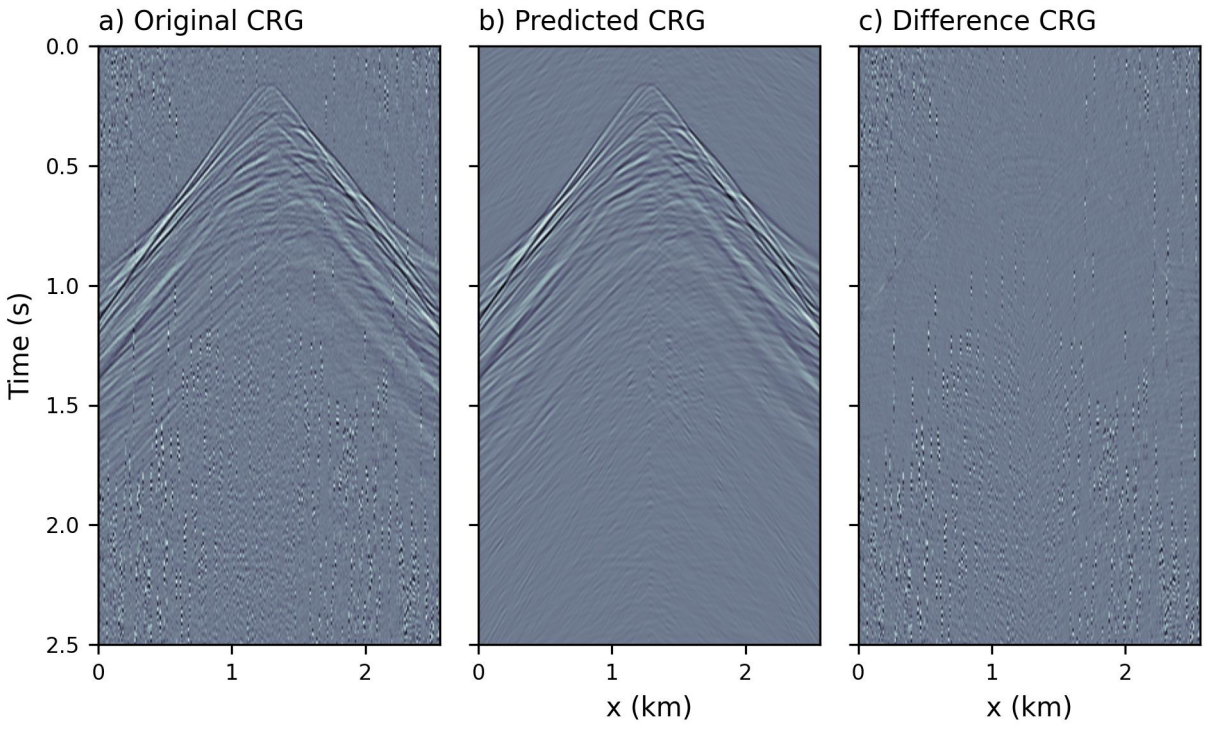


Figure 4: a) Noisy CRG. b) Deblended CRG. c) The difference panel (a-b).

Acknowledgements

We acknowledge the Signal Analysis and Imaging Group (SAIG) sponsors at the University of Alberta for supporting the stimulating research environment that allowed the preparation of this work. This publication was prepared using `SeismicJulia`, a package for reproducible seismic processing, imaging, and inversion by SAIG (https://github.com/SeismicJulia).

References

Askari, R., and S. H. Hejazi, 2015, Estimation of surface-wave group velocity using slant stack in the generalized s-transform domain: Geophysics, **80**, EN83–EN92.

Beylkin, G., 1987, Discrete radon transform: IEEE transactions on acoustics, speech, and signal processing, **35**, 162–172.

Darche, G., 1990, Spatial interpolation using a fast parabolic transform, *in* SEG Technical Program Expanded Abstracts 1990: Society of Exploration Geophysicists, 1647–1650.

Foster, D. J., and C. C. Mosher, 1992, Suppression of multiple reflections using the radon transform: Geophysics, **57**, 386–395.

Gholami, A., and M. Farshad, 2019, Fast hyperbolic radon transform using chirp-z transform: Digital Signal Processing, **87**, 34–42.

Gholami, A., and T. Zand, 2017, Fast ℓ1-regularized radon transforms for seismic data processing: Digital Signal Processing, **71**, 83–94.

Hampson, D., 1986, Inverse velocity stacking for multiple elimination, *in* SEG Technical Program Expanded Abstracts 1986: Society of Exploration Geophysicists, 422–424.

Herrmann, P., T. Mojesky, M. Magesan, and P. Hugonnet, 2000, De-aliased, high-resolution radon transforms: SEG International Exposition and Annual Meeting, SEG, SEG–2000.

Ibrahim, A., and M. D. Sacchi, 2014, Simultaneous source separation using a robust radon transform: Geophysics, **79**, V1–V11.

Kostov, C., 1990, Toeplitz structure in slant-stack inversion, *in* SEG Technical Program Expanded Abstracts 1990: Society of Exploration Geophysicists, 1618–1621.

Luo, Y., J. Xia, R. D. Miller, Y. Xu, J. Liu, and Q. Liu, 2009, Rayleigh-wave mode separation by high-resolution linear radon transform: Geophysical Journal International, **179**, 254–264.

Proakis, J. G., 2001, Digital signal processing: principles algorithms and applications: Pearson Education India.

Rabiner, L. R., R. W. Schafer, and C. M. Rader, 1969, The chirp z-transform algorithm and its application: Bell System Technical Journal, **48**, 1249–1292.

Radon, J., 1917, Über die bestimmung von funktionen durch ihre integralwerte längs gewisser mannigfaltigkeiten: Berichte über die Verhandlungen der Sächsischen Akademie der Wissenschaften zu Leipzig, Mathematisch-Physische Klasse, **69**, 262–277. (In German; English translation: "On the determination of functions from their integrals along certain manifolds" (IEEE Trans. Med. Imaging, 1986).).

Sacchi, M. D., and M. Porsani, 1999, Fast high resolution parabolic radon transform, *in* SEG Technical Program Expanded Abstracts 1999: Society of Exploration Geophysicists, 1477–1480.

Sacchi, M. D., and T. J. Ulrych, 1995, High-resolution velocity gathers and offset space reconstruction: Geophysics, **60**, 1169–1177.

Stoffa, P. L., P. Buhl, J. B. Diebold, and F. Wenzel, 1981, Direct mapping of seismic data to the domain of intercept time and ray parameter—a plane-wave decomposition: Geophysics, **46**, 255–267.

Tatham, R. H., J. W. Keeney, and I. Noponen, 1983, Application of the tau-p transform (slant-stack) in processing seismic reflection data: Exploration Geophysics, **14**, 163–172.

Trad, D. O., T. J. Ulrych, and M. D. Sacchi, 2002, Accurate interpolation with high-resolution time-variant radon transforms: Geophysics, **67**, 644–656.

Treitel, S., P. Gutowski, and D. Wagner, 1982, Plane-wave decomposition of seismograms: Geophysics, **47**, 1375–1401.

Yilmaz, Ö., 1989, Velocity-stack processing: Geophysical Prospecting, **37**, 357–382.